JUEE

Journal of Urban and Environmental Engineering, v.10, n.1, p.003-010

ISSN 1982-3932
doi: 10.4090/juee.2016.v10n1.003010

Journal of Urban and Environmental Engineering

www.journal-uee.org

RAINFALL ANALYSIS IN KLANG RIVER BASIN USING CONTINUOUS WAVELET TRANSFORM

Celso A. G. Santos[1*], Richarde M. Silva[2] and Seyed Ahmad Akrami[3]

[1]*Department of Civil and Environmental Engineering, Federal University of Paraíba, Brazil*
[2]*Department of Geosciences, Federal University of Paraíba, Brazil*
[3]*Civil and Structural Engineering Department, Universiti Kebangsaan Malaysia (UKM), Bangi, Malaysia*

Received 12 June 2015; received in revised form 26 December 2015; accepted 11 January 2015

Abstract: The rainfall characteristics within Klang River basin is analyzed by the continuous wavelet transform using monthly rainfall data (1997–2009) from a raingauge and also using daily rainfall data (1998–2013) from the Tropical Rainfall Measuring Mission (TRMM). The wavelet power spectrum showed that some frequency components were presented within the rainfall time series, but the observed time series is short to provide accurate information, thus the daily TRMM rainfall data were used. In such analysis, two main frequency components, *i.e.*, 6 and 12 months, showed to be present during the entire period of 16 years. Such semiannual and annual frequencies were confirmed by the global wavelet power spectra. Finally, the modulation in the 8–16-month and 256–512-day bands were examined by an average of all scales between 8 and 16 months, and 256 and 512 days, respectively, giving a measure of the average monthly/daily variance versus time, where the periods with low or high variance could be identified.

Keywords: Rainfall data; multiscale analysis; wavelet; Klang River

[*] Correspondence to: Celso A. G. Santos, Tel.: +55 83 3216 7684 Ext 27; Fax: +55 83 3216 7684 Ext 23.
E-mail: celso@ct.ufpb.br

INTRODUCTION

Rainfall is an important climate factor, which has significant impacts on agricultural production and national economic development (Kuang *et al.*, 2000). The Klang River basin covers a larger area, and then a good understanding of the seasonal and annual rainfall characteristics and variation trends in the basin is essential.

The wavelet transform theoretical development was in 1984 by Grossman & Morlet (1984), and since then it has attracted much attention and it is well used in signal processing as an alternative to the Fourier Transform (FT) in preserving local, non-periodic, multiscaled phenomena. Its advantage over classical spectral analysis is because it allows analyzing different scales of temporal variability and it does not need a stationary series. Therefore, it is appropriate to analyze unregular distributed events and time series that contain nonstationary power at many different frequencies, which turns it suitable for analyzing localized variations of power within a time series. Several applied fields are using wavelets, *e.g.*, acoustics, astronomy, signal processing and geophysics (Farge, 1992; Torrence & Compo, 1998; Graps, 1995; Smith *et al.*, 1998; Santos & Ideião, 2006; Braga & Santos, 2010; Santos & Freire, 2012; Santos *et al.*, 2013; Santos & Morais, 2013; Akrami *et al.*, 2014; Nourani *et al.*, 2014; Santos *et al.*, 2001, 2003, 2013, 2014a, 2014b).

The following sections describe the wavelet transform, the rainfall data of Klang River basin, and then the application of wavelet to such data using the program developed by Torrence & Compo (1998).

WAVELET TRANSFORM

Mathematical transformations are intended to obtain further information from a signal that is not readily available in its raw format. There are several transformations that can be applied, among which the Fourier transforms are probably the most popular. In order to maintain time and frequency localization in a signal analysis, one possibility would be to do a Windowed Fourier Transform (WFT), using a certain window size and sliding it along in time, computing the Fast Fourier Transform (FFT) at each time using only the data within the window. This could solve the frequency localization problem, but would still be dependent on the window size used. Another point to be observed is that the WFT relies on the assumption that the signal can be decomposed into sinusoidal components.

Thus, to measure the stationarity of a time series is necessary to calculate the running variance using a fixed-width window. Despite the disadvantage of using a fixed-width window, the analysis could be repeated

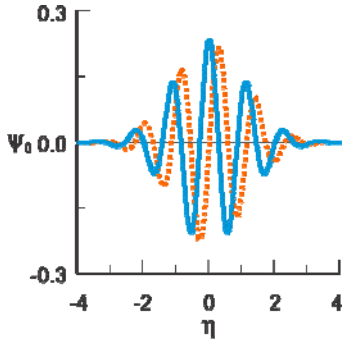

Fig. 1 Morlet wavelet base with frequency $\omega_0 = 6.0$, in which the real part is in solid line and imaginary part is in dashed line.

with a variety of window widths. By smoothly varying the window width, a picture of the changes in variance versus both time and window width could be built. The problem with this technique is the simple "boxcar" shape of the window function that introduces edge effects such as ringing. Using such a black-box-car, there will be no information on what is going on within the box, but only recover the average energy (Torrence & Compo, 1998).

These problems are solved with wavelet analysis attempts by decomposing or transforming a one-dimensional time series into a diffuse two-dimensional time-frequency image, simultaneously. It means that it is possible to get information on both the amplitude of any "periodic" signals within the series, and how this amplitude varies with time.

An example of a basic wave, of finite duration and with a specific frequency, is shown in **Fig. 1** (the Morlet wavelet). Such a shape could be used as a window function for the analysis of variance. This wavelet has the advantage of incorporating a wave of a certain period, as well as being finite in extent.

For example, if we could assume that the total width of this wavelet is about 10 years, it would be possible to find the correlation between this curve and the first 10 years of our time series. This single number would give a measure of the projection of this wave on the data during these first 10 years, *i.e.* how much [amplitude] does the 10-year period resemble a wave of this width [frequency]. By sliding this wavelet along the time series, a new time series of the projection amplitude versus time can be constructed. As for the "scale" of the wavelet, it can be varied by changing its width. This is the advantage of wavelet analysis over a moving Fourier spectrum. For a window of a certain width, the sliding FFT is fitting different numbers of waves; *i.e.*, there can be many high-frequency waves within a window, while the same window can only contain a few low-frequency waves. The wavelet analysis always uses a wavelet of the exact same shape, only the size scales up or down with the size of the window. In practice, the Morlet wavelet shown in **Fig. 1** is defined as the product of a complex exponential wave and a Gaussian envelope:

$$\Psi_0(\eta) = \pi^{-1/4} e^{i\omega_0 \eta} e^{-\eta^2/2} \quad (1)$$

where $\Psi_0(\eta)$ is the wavelet value at nondimensional time η, and ω_0 is the nondimensional frequency, equal to 6 in this study. This is the basic wavelet function, but it will be now needed some way to change the overall size as well as slide the entire wavelet along in time. Thus, the "scaled wavelets" are defined as:

$$\Psi\left[\frac{(n'-n)\delta t}{s}\right] = \left(\frac{\delta t}{s}\right)^{1/2} \Psi_0\left[\frac{(n'-n)\delta t}{s}\right] \quad (2)$$

where s is the "dilation" parameter used to change the scale, and n is the translation parameter used to slide in time. The factor of $s^{-1/2}$ is a normalization to keep the total energy of the scaled wavelet constant.

We are given a time series X, with values of x_n, at time index n. Each value is separated in time by a constant time interval δt. The wavelet transform $W_n(s)$ is just the inner product (or convolution) of the wavelet function with the original time series:

$$W_n(s) = \sum_{n'=0}^{N-1} x_{n'} \Psi * \left[\frac{(n'-n)\delta t}{s}\right] \quad (3)$$

where the asterisk (*) denotes complex conjugate.

The above integral can be evaluated for various values of the scale s (multiples of the lowest possible frequency), as well as all values of n between the start and end dates. A two-dimensional picture of the variability is constructed by plotting the wavelet amplitude and phase. Then, a time series can be decomposed into time-frequency phase space using a mother wavelet. The actual computation of the wavelet transform can be done by the following algorithm (Torrence & Compo, 1998): (a) choose a mother wavelet; (b) find the FT of the mother wavelet; (c) find the FT of the time series; (d) choose a minimum scale s_0, and all other scales; (e) for each scale, do:

• Using **Eq. (4)**, or whatever is appropriate for the mother wavelet in use, compute the daughter wavelet at that scale:

$$\Psi(s\omega_k) = \left(\frac{2\pi s}{\delta t}\right)^{1/2} \hat{\Psi}_0(s\omega_k) \quad (4)$$

where the ^ indicates the FT.

• Normalize the daughter wavelet by dividing by the square-root of the total wavelet variance (the total of Ψ^2 should then be one, thus preserving the variance of the time series);

• Multiply by the FT of your time series;

• Using **Eq. (5)**, inverse transform back to real space;

$$W_n(s) = \sum_{k=0}^{N-1} \hat{x}_k \hat{\Psi} * (s\omega_k) e^{i\omega_k n \delta t} \quad (5)$$

where ω_k is the angular frequency, equal to $2\pi k/N\delta t$ for $k \le N/2$ or equal to $-2\pi k/N\delta t$ for $k > N/2$. It is possible to compute the wavelet transform in the time domain using **Eq. (3)**. However, it is much simpler to use the fact that the wavelet transform is the convolution between the two functions x and Ψ, and to carry out the wavelet transform in Fourier space using the FFT; and (f) make a contour plot.

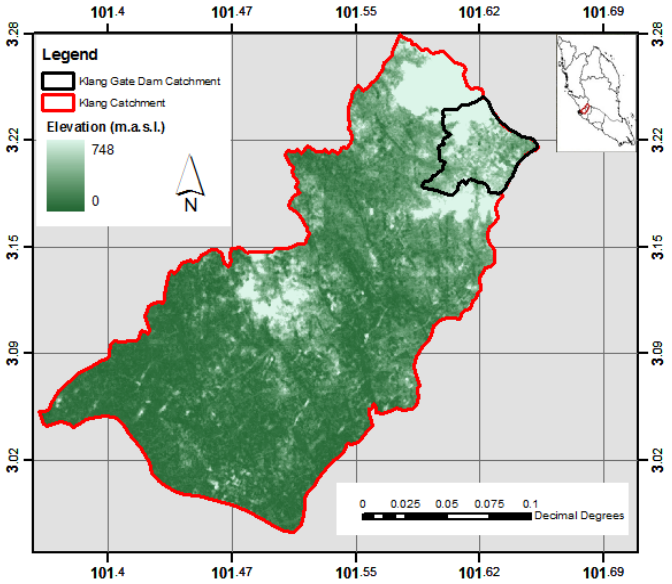

Fig. 2 The Klang River and the Klang Gate Dam basins, Malaysia.

RAINFALL DATA

The Klang River basin is located to the west coast of Malaysian Peninsular and engulfs the federal territory of Kuala Lumpur and some parts of the state of Selangor (**Fig. 2**). The study area is the most densely populated area in the country with an estimated population of over 3.7 million (about 18% of the national population). The basin has an annual population growth rate of approximately 5% and land use is dominated by urban residential development (44%), forest reserves (34%), agriculture (15%) and commercial/industry zones (7%). Urbanization and industrialization in the river basin have been rapidly replacing major portions of agricultural and ex-mining land. As a result of the extensive and rapid urban development in the basin area, problems have emerged in the form of over bank floods and flash floods due to clogged drainage systems and changes of the river physical environment. This has prompted the commissioning of a number of flood mitigation and river environment enhancement programs as the problems and the associated social and economic costs have been escalating with more urbanization (Earth Observation Centre UKM Malaysia, 2013).

The Klang River, with 120 km length, originates from the Main Range (at an altitude of about 1330 m) and about 25 km to the north of Kuala Lumpur. This river finally pours into the sea at the Strait of Melaka. This river also flows through a region with a dense

population. Eleven tributaries comprise the water of Klang River. Some of these tributaries are Ampang, Bunus, Damansara, Gombak, and Batu. Klang River's upper basin is a fairly mountainous with a steep slope. The Klang valley's latitude is 3°14′ N and its longitude is 101°45′ E (EOC, 2013).

Klang River basin is the most developed region in Malaysia, especially, in the city of Kuala Lumpur. However, runoffs have become a serious problem in this region during the past decade. The floods occurred in early 21st century showed that the infrastructure, especially the channels, which were constructed in this region were not enough to cater for the flood flows. This situation is more complicated in the areas where the flood has to pass where exists a bridge, *i.e.* Tun Perak bridge blocks the flow of flood. Heavy rainfall and runoffs have also caused serious problems in areas such as Sungai Ampang and the upper Sungai Klang. The most critical regions are Sungai Batu and Sungai Gombak which are located on the north-west of the catchment. The region known as Masjid Jamek is the confluence of Sungai Klang and Sungai Gombak. It has been estimated that the occurrence of heavy rainfall like those in early 21st century, which caused damages in areas like Jalan Tun Perak, Jalan Kuching, High Court Complex, City Hall Car Park, Masjid Jamek, would be catastrophic (EOC, 2013). The map in **Fig. 2** provides more information on Klang River, Klang Dam Catchment, Klang Gate Dam, etc.

The rainfall data set of Klang River was based on Klang Gates Dam data from the year 1997 to 2008 (**Fig. 3a**), which present a mean, maximum, minimum and standard deviation values equal to 232.45 mm (r_{mean}), 662.80 mm (r_{max}), 9.60 mm (r_{min}) and 116.54 mm (r_{std}), respectively.

RESULTS AND DISCUSSION

Wavelet analysis was chosen, besides the other reasons and advantages described earlier, because applications such as standard Fourier Transform analysis to a time series should be only attempted when the time series

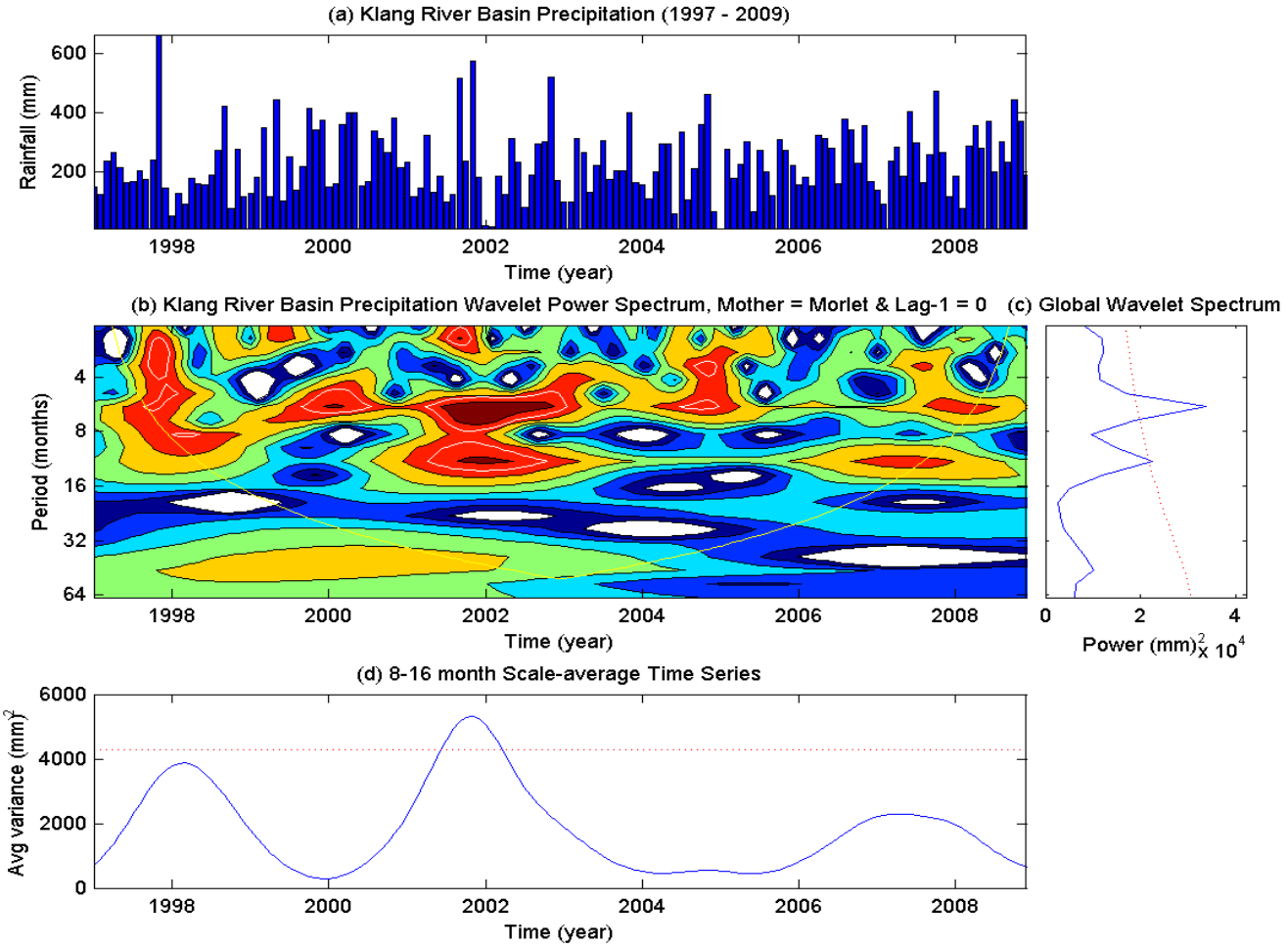

Fig. 3 (a) The Klang River basin monthly rainfall hyeotograpgh. (b) The wavelet power spectrum using Morlet mother-wavelet. The contour levels are chosen so that 75%, 50%, 25%, and 5% of the wavelet power is above each level, respectively. Region below the yellow line is the cone of influence, where zero padding has reduced the variance. White contour is the 5% significance level, using a white-noise background spectrum. (c) The global wavelet power spectrum (blue line). The dashed line is the 5% significance level for the global wavelet spectrum. (d) Scale-average wavelet power over the 8–16-month band for the monthly rainfall. The dashed line is the 95% confidence level assuming white-noise.

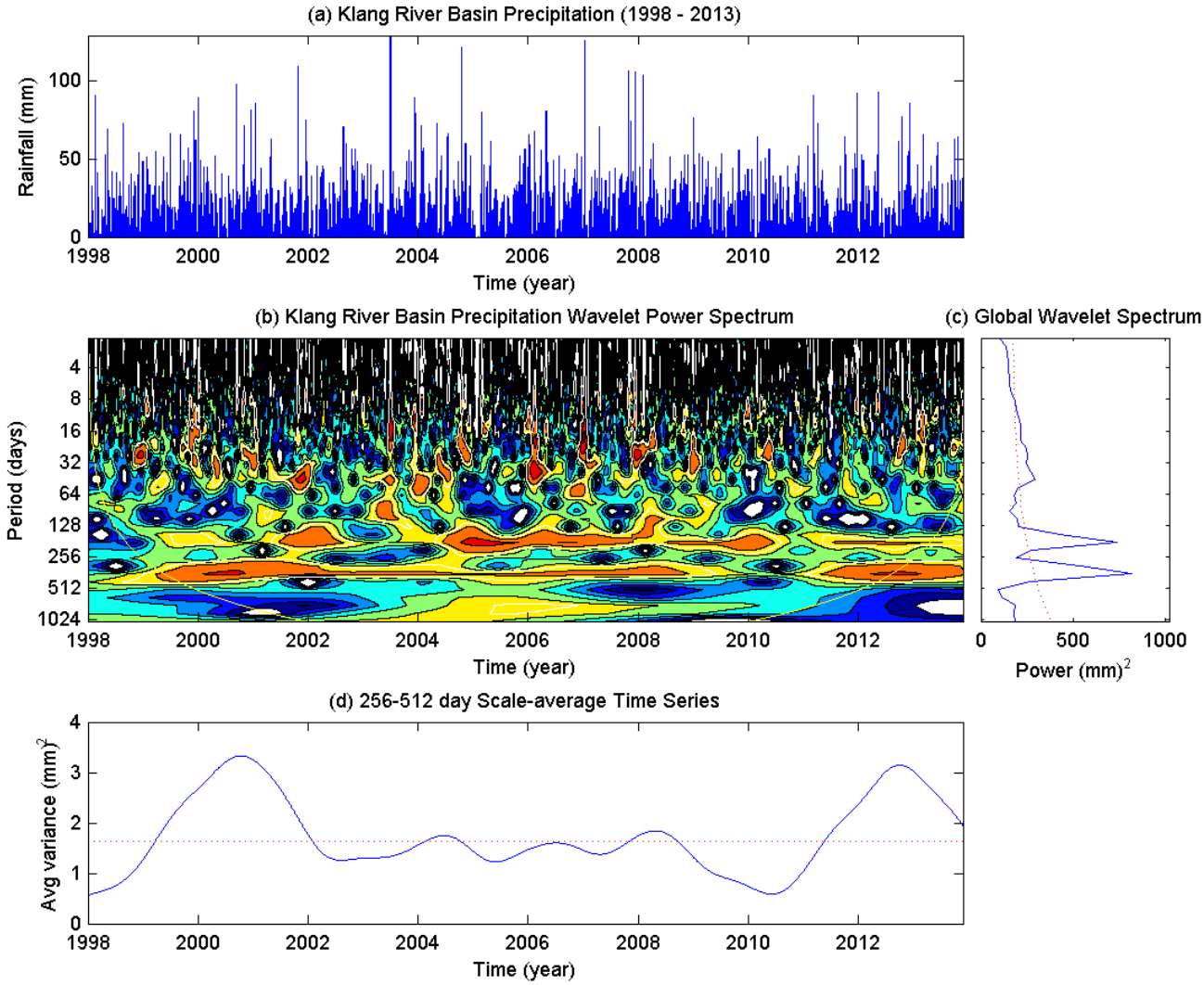

Fig. 4 (a) The Klang River basin daily TRMM rainfall hyetograph. (b) The wavelet power spectrum using Morlet mother-wavelet. The contour levels are chosen so that 75%, 50%, 25%, and 5% of the wavelet power is above each level, respectively. Region below the yellow line is the cone of influence, where zero padding has reduced the variance. White contour is the 5% significance level, using a white-noise background spectrum. (c) The global wavelet power spectrum (blue line). The dashed line is the 5% significance level for the global wavelet spectrum. (d) Scale-average wavelet power over the 256–512-day band for the daily rainfall. The dashed line is the 95% confidence level assuming white-noise.

fulfils two important characteristics: (1) stationarity; *i.e.*, that no changes in the mean, variance, etc., occur throughout the time series; and (2) that the time series can be described as the summation of different periodic components (described by simple harmonic functions) for the whole period. The time series described here do not fulfil both requirements. In fact, earth sciences time series are usually nonstationary and present trends of the mean value, changes in the variability for certain periods (Silva *et al.*, 2015a). Furthermore, precipitation time series may present unregular distributed events with nonstationary power over many different frequencies. Thus, their intrinsic temporal structure is not well represented by the superposition of a few frequency components as derived in a usual Fourier analysis. The periodic oscillation of rainfall variation and the points of abrupt change at different time scales along the time series are discovered. The results indicate that there are obvious periodic oscillations of 8–12 years and 4–6 years for the seasonal and annual rainfalls variation.

Wavelet power spectrum

For the monthly distributed data, the parameters for the wavelet analysis are set as $\delta t = 1$ month and $s_0 = 2$ months because $s = 2\delta t$; $\delta j = 0.25$ to do 4 sub-octaves per octave; and $j_1 = 6/\delta j$ in order to do 6 powers-of-two with δj sub-octaves each; and for the daily distributed data, the parameters are set as $\delta t = 1$ day and $s_0 = 2$ days because $s = 2\delta t$; $\delta j = 0.25$ to do 4 sub-octaves per octave; and $j_1 = 10/\delta j$ in order to do 10 powers-of-two with δj sub-octaves each.

Figure 3b shows the power (absolute value squared) of the wavelet transform for the monthly rainfall in Klang River basin presented in **Fig. 3a**, which is a record of the period between 1997 and 2008. The spectrum in **Fig. 3b** gives information on the relative power at a certain scale and a certain time and it shows the actual oscillations of the individual wavelets, rather than just their magnitude. It is possible to note that there is more concentration of power between the 4–16-month band, but unfortunately it is not clear when each frequency occurs. Thus, we make use of TRMM rainfall data in order to explain better such oscillations (**Figs 4**–**5**). **Figure 4a** shows the TRMM daily rainfall record of the period of 1998−2013 (r_{mean} = 231.32 mm, r_{max} = 435.72 mm, r_{min} = 7.65 mm, r_{std} = 82.51 mm) and the power of the wavelet transform is shown in **Fig. 4b**, in which it is clear to note the two frequencies, one between the 128–256-day band and another between the 256–512-day band, are present almost during the whole time series. Those frequencies correspond respectively to semiannual and annual signals, which are confirmed by the global wavelet spectrum in **Fig. 4c**. Such signals are not clear in **Fig. 3c**., probably due to the data quality rather than true signal information. The variance of power in 8–16-month band (**Fig. 3d**) shows the dry and wet years in an annual basis; *i.e.*, when the power decreases substantially in this band, it means a dry year and when the power is maximum means a wet year. Only one wet period can be identified in 2001, but **Fig. 4d** shows with more precision wet periods in 1999–2001 and in 2011–2013 within the 256–512-day band.

The region below the yellow line in those figures (**Figs 3b and 4b**) is the cone of influence, where zero padding has reduced the variance. Because we are dealing with finite-length time series, errors will occur at the beginning and end of the wavelet power spectrum. Torrence & Compo (1998) explain that one solution is to pad the end of the time series with zeroes before applying the wavelet transform and then remove them afterward. Here the time series is padded with sufficient zeroes to bring the total length N up to the next-higher power of two, thus limiting the edge effects and speeding up the Fourier Transform. Padding with zeroes introduces discontinuities at the endpoints and decreases the amplitude near the edges as going to larger scales, since more zeroes enter the analysis. The cone of influence is the region of the wavelet spectrum in which edge effects become important and is defined as the e-folding time for the autocorrelation of wavelet power at each scale. The peaks within these regions have presumably been reduced in magnitude due to the zero padding. Thus, it is unclear whether the decrease in any band power in this cross-hatched region is a true decrease in variance or an artifact of the padding. Note also that for cyclic series, there is no need to pad with zeroes, and there is no cone of influence (Santos *et al.*, 2013).

The white contour in the same figure is the 5% significance level, using a white-noise background spectrum. Many geophysical time series can be modeled as either white-noise or red-noise. A simple model for red-noise is the univariate lag-1 autoregressive process. The lag-1 is the correlation between the time series and itself, but shifted (or lagged) by one time unit. In this present case, this would be a shift of one day (**Fig. 4**) or one month (**Figs 3** and **5**). The lag-1 measures the persistence of an anomaly from one day/month to the next. The true lag-1 α can be computed by an approximation using $\alpha = (\alpha_1 + \alpha_2^{1/2})/2$, where α_1 is the lag-1 autocorrelation and α_2 is the lag-2 autocorrelation, which is the same as lag-1 but just shifted by two points instead of one. The time series studied show α_1 less than 0.4, then according to Santos *et al.* (2013) it is better to test them to white-noise ($\alpha_1 = 0.0$).

The null hypothesis is defined for the wavelet power spectrum as assuming that the time series has a mean power spectrum; if a peak in the wavelet power spectrum is significantly above this background spectrum, then it can be assumed to be a true feature with a certain percent confidence. For definitions, "significant at the 5% level" is equivalent to "the 95% confidence level," and implies a test against a certain background level, while the "95% confidence interval" refers to the range of confidence about a given value. The 95% confidence implies that 5% of the wavelet power should be above this level.

Global wavelet power spectrum

The semiannual and annual frequencies (periodicity at 6 and 12 months) of these time series are confirmed by an integration of power over time (**Figs 3c**, **4c** and **5c**), which show two significant peaks above the 95% confidence level for the global wavelet spectrum, assuming white-noise, represented by the dashed lines. However, **Fig. 4c** also presents significant peaks (at the 5% level) centered in the 8–64-day band, which correspond to pulses of highly significant power within such a band (one week up to two months). These global wavelet spectra provide an unbiased and consistent estimation of the true power spectrum of the time series, and thus they are a simple and robust way to characterize the time series variability.

Scale-average time series

The scale-average wavelet power is a time series of the average variance in a certain band, in this case 8–16-month band (**Fig. 3d**) and 256–512-day band (**Fig. 4d**), used to examine modulation of one frequency by another within the same time series. These figures are

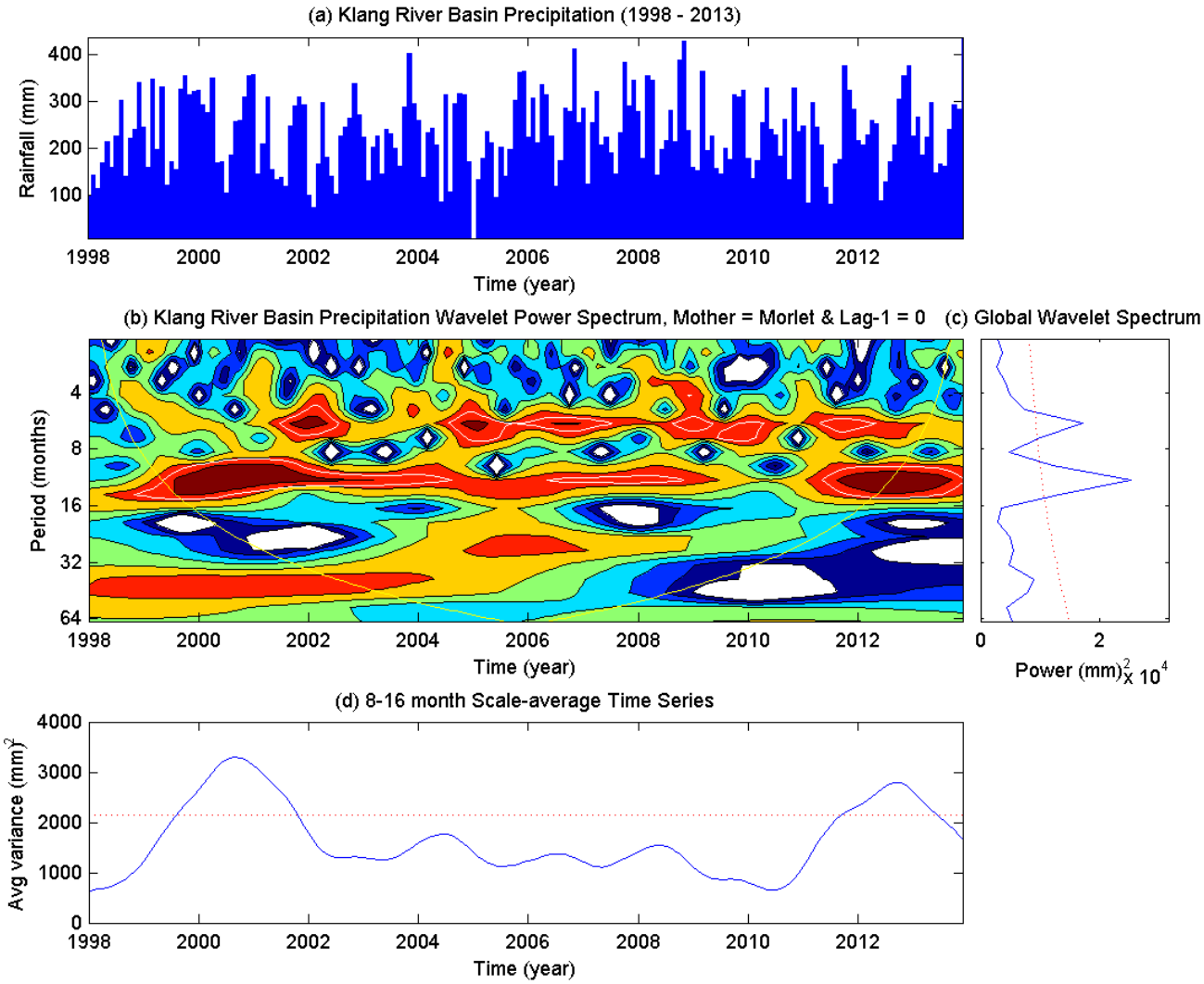

Fig. 5 (a) The Klang River basin monthly TRMM rainfall hyetograph. (b) The wavelet power spectrum using Morlet mother-wavelet. The contour levels are chosen so that 75%, 50%, 25%, and 5% of the wavelet power is above each level, respectively. Region below the yellow line is the cone of influence, where zero padding has reduced the variance. White contour is the 5% significance level, using a white-noise background spectrum. (c) The global wavelet power spectrum (blue line). The dashed line is the 5% significance level for the global wavelet spectrum. (d) Scale-average wavelet power over the 8–16-month band for the monthly rainfall. The dashed line is the 95% confidence level assuming white-noise.

made respectively by the average of **Figs 3b** and **4b** over all scales between 8 and 16 months, and between 256 and 512 days, respectively, which gives a measure of the average year variance versus time. The variance plot shows distinct periods when the rainfall variance was low or high as described before.

Figure 3d shows just one wet period around 2012, but **Figs 4d** and **5d** clarify that the wet periods can be found from 1999 up to the end of 2001, and another starting in 2011.

CONCLUSION

In order to study the variability of the rainfall time series in Klang River basin, TRMM data are used and the wavelet analysis is applied. The wavelet power spectrum using monthly data from a rainfall gauge within the basin shows some power concentration and the TRMM daily data reveals the location of such power concentration, of which two main frequency components can be found, *i.e.* semiannual and annual periodicities of such event, which is confirmed by the peak of the integration of transform magnitude vectors over time. The periods with low variance in such bands can be identified by the average of the all scales within the selected bands. The annual frequency disappears in 2010, and the semiannual frequency is low until 2001 and in 2003. The monthly wavelet transform analysis using the TRMM also confirms such results (**Fig. 5**). The TRMM shows to be accurate when compared to the rainfall data from a conventional gauge and very convenient for hydrological studies as cluster analysis (Brito Neto *et al.*, 2015), time series trends (Santos *et al.*, 2015; Silva *et al.*, 2015a; 2015b) and erosion (Farias & Santos, 2014; Santos *et al.*, 2014d; 2015) since it is a continuous daily rainfall time series since 1998.

Acknowledgment The authors wish to thank Dr. Christopher Torrence of Exelis Visual Information Solutions – Pearl East Circle, Colorado, for providing the wavelet analysis computer program and material.

REFERENCES

Akrami, S.A., El-shafie, A., Naseri, M. & Santos, C.A.G. (2014) Rainfall data analyzing using moving average (MA) model and wavelet multi-resolution intelligent model for noise evaluation to improve the forecasting accuracy. *Neural Comp. & Appl.*, **25**(7/8), 1853–1861. doi: 10.1007/s00521-014-1675-0

Braga, I.Y.L.G. & Santos, C.A.G. (2010) Viability of rainwater use in condominiums based on the precipitation frequency for reservoir sizing analysis. *J. Urban Environ. Engng*, **4**(1), 23–28. doi: 10.4090/juee.2010.v4n1.023028

Brito Neto, R.T., Santos, C.A.G., Mulligan, K. & Barbato, L. (2015) Spatial and temporal water-level variations in the Texas portion of the Ogallala Aquifer. *Nat. Hazards*, **80**(1), 351–365. doi: 10.1007/s11069-015-1971-8

EOC – Earth Observation Centre (2013) Universiti Kebangsaan Malaysia (UKM), Malaysia 2013.

Farge, M. (1992) Wavelet transforms and their applications to turbulence. *Ann. Rev. Fluid Mech.*, **24**, 395–457. doi: 10.1146/annurev. fl.24.010192.002143

Farias, C.A.S. & Santos, C.A.G. (2014) The use of Kohonen neural networks for runoff-erosion modeling. *J. Soils Sedim.*, **14**(7), 1242-1250. doi: 10.1007/s11368-013-0841-9

Graps, A. (1995) An introduction to wavelets, *IEEE Computational Sci. and Engng*, **2**(2), 50-61. doi: 10.1109/99.388960

Grossman, A. & Morlet, J. (1984) Decomposition of Hardy functions into square integrable wavelets of constant shape. *SIAM J. Math. Anal.*, **15**(4), 723-736. doi: 10.1137/0515056

Kuang, Z., Ji, Z. Z., Lin, Y. H., (2000) Wavelet analysis of rainfall data in North China. *Climatic Environ. Res.*, **5**(3), 312–317.

Nourani, V., Baghanam, A.H., Adamowski, J., Kisi, O. (2014) Applications of hybrid wavelet–Artificial Intelligence models in hydrology: A review. *J. Hydrol*. **514**, 358-377. doi: 10.1016/j.jhydrol. 2014.03.057

Santos, C.A.G. & Freire, P.K.M.M. (2012) Analysis of precipitation time series of urban centers of northeastern Brazil using wavelet transform. *Int. J. Environ. Chem. Ecol. Geol. Geophys. Engng*, **6**(7), 64–69.

Santos, C.A.G. & Ideião, S.M.A. (2006) Application of the wavelet transform for analysis of precipitation and runoff time series. *IAHS Publ.*, **303**, 431–439.

Santos, C.A.G. & Morais, B.S. (2013) Identification of precipitation zones within São Francisco River basin (Brazil) by global wavelet power spectra. *Hydrol. Sci. J.*, **58**(4), 789–796. doi: 10.1080/02626667.2013.778412

Santos, C.A.G. & Silva, G.B.L. (2014a) Daily streamflow forecasting using a wavelet transform and artificial neural network hybrid models. *Hydrol. Sci. J.*, **59**(2), 1–13. doi: 10.1080/02626667.2013. 800944

Santos, C.A.G., Freire, P.K.M.M. & Torrence, C. (2013) A transformada wavelet e sua aplicação na análise de séries hidrológicas. *Rev. Bras. Rec. Hídric.*, **18**(3), 271–280.

Santos, C.A.G., Freire, P.K.M.M., Silva, G.B.L. & Silva, R.M. (2014b) Discrete wavelet transform coupled with ANN for daily discharge forecasting into Três Marias reservoir. *Proc. Int. Assoc. Hydrol. Sci.*, 364, 100–105. doi: 10.5194/piahs-364-100-2014

Santos, C.A.G., Galvão, C.O. & Trigo, R.M. (2003) Rainfall data analysis using wavelet transform. *IAHS Publ.* **278**, 195–201.

Santos, C.A.G., Galvão, C.O., Suzuki, K. & Trigo, R.M. (2001) Matsuyama city rainfall data analysis using wavelet transform. *Proc. Hydraul. Engng*, Tokyo, **45**, 211–216. doi: 10.2208/ prohe.45.211

Santos, C.A.G., Silva, R.M., Moreira, M., Corte-Real, J. & Mangueira, L.R. (2015) Detecting hydro-climatic change using spatiotemporal analysis of rainfall time series in the Cobres River basin, Portugal. *Proc. Int. Assoc. Hydrol. Sci.*, **366**, 125–126. doi: 10.5194/piahs-366-125-2015

Santos, J.Y.G., Silva, R.M., Carvalho Neto, J.G., Montenegro, S.M.G.L., Santos, C.A.G. & Silva, A.M. (2014b) Assessment of land-use change on streamflow using GIS, remote sensing and a physically-based model, SWAT. *Proc. Int. Assoc. Hydrol. Sci.*, **364**, 38–43. doi: 10.5194/piahs-364-38-2014

Silva, R.M., Santos, C.A.G., Macêdo, M.L.A., Silva, L.P. & Freire, P.K.M.M. (2013) Space-time variability of rainfall and hydrological trends in the Alto São Francisco River basin. *IAHS Publ.,* **359**, 177–182.

Silva, R.M., Santos, C.A.G., Moreira, M., Corte-Real, J., Silva, V.C.L. & Medeiros, I.C. (2015a) Rainfall and river flow trends using Mann-Kendall and Sen's slope estimator statistical tests in the Cobres River basin. *Nat. Hazards*, **77**(2), 1205–1221. doi: 10.1007/s11069-015-1644-7

Silva, R.M., Santos, C.A.G., Moreira, M., Corte-Real, J. & Barbosa, R.C. (2015b) Rainfall trends over 40 years in the Cobres River basin, Portugal: variability and impacts. *Proc. Int. Assoc. Hydrol. Sci.*, **366**, 127–128. doi: 10.5194/piahs-366-127-2015

Smith, L.C., Turcitte, D.L. & Isacks, B.L. (1998) Stream flow characterization and feature detection using a discrete wavelet transform, *Hydrol. Processes*, **12**(2), 233–249. doi: 10.1002/(SICI)1099-1085(199802)12:2<233::AID-HYP573>3.0. CO;2-3

Torrence, C. & Compo, G.P. (1998) A practical guide to wavelet analysis. *Bull. Amer. Meteor. Soc.*, **79**(1), 61–78. doi: 10.1175/1520-0477(1998)079<0061:APGTWA>2.0.CO;2